

# Vibration control of laminated composite plates using embedded smart layers

J.N. Reddy<sup>†</sup> and S. Krishnan<sup>‡</sup>

*Department of Mechanical Engineering, Texas A&M University, College Station, TX 77843-3123, U.S.A.*

**Abstract.** Analytical solutions and finite element results of laminated composite plates with smart material layers embedded in them are presented in this study. The third-order plate theory of Reddy is used to study vibration suppression characteristics. The analytical solution for simply supported boundary conditions is based on the Navier solution procedure. The velocity feedback control is used. Parametric effects of the position of the smart material layers, material properties, and control parameters on the suppression time are investigated. It has been found that (a) the minimum vibration suppression time is achieved by placing the smart material layers farthest from the neutral axis, (b) using thinner smart material layers have better vibration attenuation characteristics, and, (c) the vibration suppression time is larger for a lower value of the feedback control coefficient.

**Key words:** analytical solutions; composite plates; finite element solutions; third-order plate theory; vibration control.

---

## 1. Introduction

### 1.1 Background

The phrase *smart structural system* refers to a wide variety of active material and passive structural systems (Newnham 1993). For instance, a sufficiently general system is a composite (beam, plate, shell, or any other fundamental form) with embedded or surface mounted piezoelectric or electrostrictive patches, or even layers of active materials in a laminated system Fig. 1. The literature contains many definitions of *smart* and *intelligent* structures. According to Newnham's definition, the structures with surface mounted or embedded sensors and actuators that have the capability to sense and take corrective action are referred to as smart structures. The feedback circuitry linking sensing and actuating is external to the sensor and actuator components. In fact, this precisely distinguishes a smart structural system from an intelligent structural system. Intelligent structural systems involve smart components in which the functions of sensing, feedback control, and actuating are all integrated. This type of system finds applications in aircraft wings, helicopter rotors, weapon systems, automobiles, and so on.

Two of the basic elements of a smart structural system are actuators and sensors. These sensors and actuators may be either mounted on the flexible passive structure or embedded inside it. The

---

<sup>†</sup> Distinguished Professor

<sup>‡</sup> Graduate Research Assistant

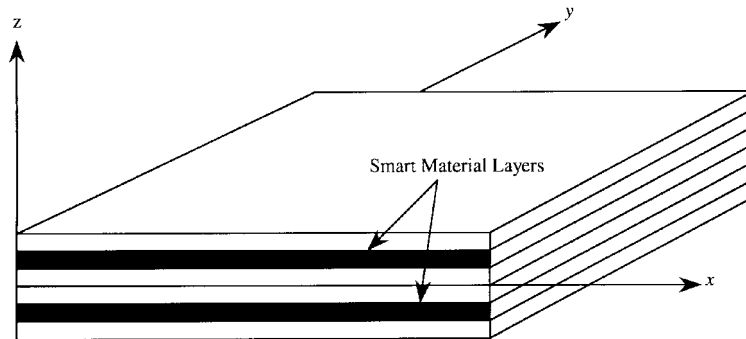


Fig. 1 Laminated composite plate with inserts of smart material layers

sensing and control of flexible structures are primarily performed with the help of discretely placed sensors and actuators.

There are a number of materials that have the capability to be used as a sensor or an actuator or both a sensor and actuator. A few examples of such materials that could be integrated with a structure to make it smart are piezoelectric materials, magnetostrictive materials, electrostrictive materials, shape memory alloys, and electro-rheological fluids. Among these materials, piezoelectric and magnetostrictive materials have the capability to serve as both sensors and actuators. Piezoelectricity (Maugin 1988) is a phenomenon in which some materials develop polarization upon application of strains. This phenomenon is observed in materials that have a non-centrosymmetric crystal structure. Examples of piezoelectric materials are Rochelle salt, quartz, and the most popular one, Lead Zirconate Titanate or PZT ( $\text{Pb}(\text{Zr,Ti})\text{O}_3$ ). Piezoelectric materials exhibit a linear relationship between the electric field and strains for low field values (up to 100 V/mm). However, the relationship is nonlinear for large fields, and the material exhibits hysteresis (Uchino 1986). Furthermore, piezoelectric materials show dielectric aging and hence lack reproducibility of strains, i.e., a drift from zero state of strain is observed under cyclic electric field conditions (Cross and Jang 1988).

Bailey and Hubbard (1985) and Crawley and Luis (1987) demonstrated the feasibility of using piezoelectric actuators for free vibration reduction of cantilever beams. A self-sensing active constrained damping layer treatment for a Euler-Bernoulli beam was studied by Yellin and Shen (1996). Baz *et al.* (1990) have investigated vibration control using shape memory alloy actuators and their characterization. Anders *et al.* (1991) have analytically demonstrated their control of sound radiation from shape memory alloy hybrid composite panels. By changing the elastic properties of the host structure, Choi *et al.* (1990) demonstrated the vibration reduction effects of electrorheological fluid actuators in a composite beam.

An ideal actuator, for distributed embedded application, must have high energy density, negligible weight, and point excitation with a wide frequency bandwidth. Terfenol-D, a magnetostrictive material, has the characteristics of being able to produce strains up to 2500  $\mu\text{m}$  and energy density as high as 25000  $\text{Jm}^{-3}$  in response to a magnetic field. Goodfriend and Shoop (1992) reviewed the material properties of Terfenol-D with regard to its use in vibration isolation. Anjanappa and Bi (1994a, b) investigated the feasibility of using embedded magnetostrictive mini actuators for smart structure applications, such as vibration suppression of beams. Bryant, Fernandez, and Wang (1993) have presented results of an experiment in which rod of magnetostrictive Terfenol-D was used in

the dual capacity of passive structural support element and an active vibration control actuator. A self-sensing magnetostrictive actuator design based on a linear model of magnetostrictive transduction for Terfenol-D was developed and analyzed by Pratt and Flatau (1995). Eda *et al.* (1995) and Krishna Murty *et al.* (1997, 1998) proposed magnetostrictive actuators that take advantage of ease with which the actuators can be embedded and remote excitation capability of magnetostrictive particles as new actuators for smart structures.

## 1.2 Present Study

Vibrations or shape control of flexible structures is achieved with the help of actuators and a control law. Many modern techniques have been developed in recent years to meet the challenge of designing controllers that suit the function under some required conditions. There have been a number of studies on vibration control of flexible structures using smart materials (Anjanappa and Bi 1994a, b, Bryant, Fernandez, and Wang 1993, Pratt and Flatau 1995, Eda *et al.* 1995, Krishna Murty *et al.* 1997, 1998, Reddy and Barbosa 2000).

In this current work vibration control of laminated composite plates is studied using the third-order plate theory of Reddy (Reddy 1984a, b, 1997), based on the formulation presented by Reddy (1999a). The third-order shear deformation theory is used. A simple negative velocity feed back control is used to actively control the dynamic response of the structure through a close-loop control. The analytical solutions are developed for simply supported boundary conditions and a displacement finite element model is used for a general plate. The effects of material properties, lamination scheme, and placement of the smart material layer on vibration suppression are investigated.

## 2. Theoretical Formulation

### 2.1 Introduction

The simplest equivalent single-layer theories are the classical laminate plate theory (CLPT) and the first-order shear deformation theory (FSDT). These theories adequately describe the kinematics of most laminated plates (Reddy 1997). However, for better inter-laminar stress distributions, higher-order theories are used. One such theory is the third-order shear deformation plate theory of Reddy (1984a, b, 1997, 1999b). In this section the complete derivation of the governing equations of the third-order plate theory for laminated plates with embedded actuating layers and velocity feedback control is presented.

Consider a symmetric laminated composite plate of  $n$  layers with the  $m^{\text{th}}$  and the  $(n-m+1)^{\text{st}}$  layers being those made of a smart material that is capable of sensing and actuating. The remaining  $n-2$  layers are made of the fiber-reinforced material that has a varying fiber orientation  $\theta$  and symmetrically disposed about the center of the plate. An illustration of a composite plate with smart material inserts is shown in Fig. 1. The assumption of symmetric lamination scheme is necessary only for the development of analytical solutions, and it can be removed for the finite element model development. In the latter case the actuating layers can be replaced with patches and they can be embedded throughout the structure as dictated by an optimization procedure.

For the sake of completeness some of the key equations of the third-order plate theory and its

finite element model are repeated here. For additional details, the reader may consult Reddy (1999a).

## 2.2 Displacement and field

The displacement field for the third-order shear deformation theory (TSDT) is of the form

$$\begin{aligned} u(x,y,z,t) &= u_0(x,y,t) + z\varphi_x(x,y,t) - c_1 z^3 \left( \varphi_x + \frac{\partial w_0}{\partial x} \right) \\ v(x,y,z,t) &= v_0(x,y,t) + z\varphi_y(x,y,t) - c_1 z^3 \left( \varphi_y + \frac{\partial w_0}{\partial y} \right) \\ w(x,y,z,t) &= w_0(x,y,t) \end{aligned} \quad (1)$$

where  $(u_0, v_0, w_0)$  denotes the displacements of a point on the plane  $z=0$ ,  $(\varphi_x, \varphi_y)$  denote the rotations of a transverse normal about the  $y$ - and  $x$ -axes, respectively, and  $c_1=4/3h^2$ .

## 2.3 Constitutive relations

Each composite lamina of the plate is assumed to behave as an orthotropic material, with its material axes oriented arbitrarily with respect to the laminate coordinates. The smart material layer can be orthotropic, but taken to be isotropic in actual calculations. The constitutive equations of each layer when referred to the laminate coordinates  $(x, y, z)$ , are

$$\begin{aligned} \begin{Bmatrix} \sigma_{xx} \\ \sigma_{yy} \\ \sigma_{xy} \end{Bmatrix}^{(k)} &= \begin{bmatrix} \bar{Q}_{11} & \bar{Q}_{12} & \bar{Q}_{16} \\ \bar{Q}_{12} & \bar{Q}_{22} & \bar{Q}_{26} \\ \bar{Q}_{16} & \bar{Q}_{26} & \bar{Q}_{66} \end{bmatrix}^{(k)} \begin{Bmatrix} \varepsilon_{xx} \\ \varepsilon_{yy} \\ \varepsilon_{xy} \end{Bmatrix} - z \begin{bmatrix} 0 & 0 & \bar{e}_{31} \\ 0 & 0 & \bar{e}_{32} \\ 0 & 0 & \bar{e}_{36} \end{bmatrix}^{(k)} \begin{Bmatrix} 0 \\ 0 \\ H_z \end{Bmatrix} \\ \begin{Bmatrix} \sigma_{yz} \\ \sigma_{xz} \end{Bmatrix}^{(k)} &= \begin{bmatrix} \bar{Q}_{44} & \bar{Q}_{45} \\ \bar{Q}_{45} & \bar{Q}_{55} \end{bmatrix}^{(k)} \begin{Bmatrix} \gamma_{yz} \\ \gamma_{xz} \end{Bmatrix} + \begin{bmatrix} \bar{e}_{14} & \bar{e}_{24} & 0 \\ \bar{e}_{15} & \bar{e}_{25} & 0 \end{bmatrix}^{(k)} \begin{Bmatrix} 0 \\ 0 \\ H_z \end{Bmatrix} \end{aligned} \quad (2)$$

where  $\bar{Q}_{ij}$  are the transformed stiffnesses,  $\bar{e}_{ij}$  are the transformed moduli of the actuating/sensing material, which in the present study is taken to be a magnetostrictive material, and  $Q_{ij}^{(k)}$  are the plane stress-reduced stiffnesses and  $e_{ij}^{(k)}$  are the piezoelectric or magnetostrictive coupling moduli of the  $k^{th}$  lamina, if it is not a structural layer. The  $d_{ij}$  are the coupling coefficients that couple the elastic structure with the smart material. Here  $\theta$  is the angle measured counter-clockwise from the  $x$ -coordinate to the  $x_1$ -coordinate. For the structural part of the composite structure the electric field intensity  $H_z$  should be excluded in Eq. (2). The coefficients  $Q_{ij}^{(k)}$  are known in terms of the engineering constants of the  $k^{th}$  layer (see Reddy 1999a, b).

## 2.4 Equations of motion

The equations of motion of the third-order plate theory are

$$\frac{\partial N_{xx}}{\partial x} + \frac{\partial N_{xy}}{\partial y} = I_o \frac{\partial^2 u_0}{\partial t^2} + J_1 \frac{\partial^2 \varphi_x}{\partial t^2} - c_1 I_3 \frac{\partial^2}{\partial t^2} \left( \frac{\partial w_0}{\partial x} \right)$$

$$\begin{aligned}
\frac{\partial N_{xy}}{\partial x} + \frac{\partial N_{yy}}{\partial y} &= I_o \frac{\partial^2 v_0}{\partial t^2} + J_1 \frac{\partial^2 \varphi_y}{\partial t^2} - c_1 I_3 \frac{\partial^2}{\partial t^2} \left( \frac{\partial w_0}{\partial y} \right) \\
\frac{\partial \bar{Q}_x}{\partial x} + \frac{\partial \bar{Q}_y}{\partial y} + c_1 \left( \frac{\partial^2 P_{xx}}{\partial x^2} + 2 \frac{\partial^2 P_{xy}}{\partial x \partial y} + \frac{\partial^2 P_{yy}}{\partial y^2} \right) + q &= \\
I_0 \frac{\partial^2 w_0}{\partial t^2} - c_1^2 I_6 \frac{\partial^2}{\partial t^2} \left( \frac{\partial^2 w_0}{\partial x^2} + \frac{\partial^2 w_0}{\partial y^2} \right) + c_1 \left[ I_3 \frac{\partial^2}{\partial t^2} \left( \frac{\partial u_0}{\partial x} + \frac{\partial v_0}{\partial y} \right) + J_4 \frac{\partial^2}{\partial t^2} \left( \frac{\partial \varphi_x}{\partial x} + \frac{\partial \varphi_y}{\partial y} \right) \right] \\
\frac{\partial \bar{M}_{xx}}{\partial x} + \frac{\partial \bar{M}_{xy}}{\partial y} - \bar{Q}_x &= \frac{\partial^2}{\partial t^2} \left( J_1 u_0 + K_2 \varphi_x - c_1 J_4 \frac{\partial w_0}{\partial x} \right) \\
\frac{\partial \bar{M}_{xy}}{\partial x} + \frac{\partial \bar{M}_{yy}}{\partial y} - \bar{Q}_y &= \frac{\partial^2}{\partial t^2} \left( J_1 v_0 + K_2 \varphi_y - c_1 J_4 \frac{\partial w_0}{\partial y} \right)
\end{aligned} \quad (3)$$

where

$$\begin{aligned}
\bar{M}_{\alpha\beta} &= M_{\alpha\beta} - c_1 P_{\alpha\beta}, \quad \bar{Q}_\alpha = Q_\alpha - 3c_1 R_\alpha \\
I_i &= \sum_{k=1}^N \int_{z_k}^{z_{k+1}} \rho^{(k)}(z) z^i dz \quad (i=0, 1, 2, \dots, 6) \\
J_i &= I_i - c_1 I_i, \quad K_2 = I_2 - 2c_1 I_4 + c_1^2 I_6, \quad c_1 = \frac{4}{3h^2}
\end{aligned} \quad (4)$$

and  $(N_{xx}, N_{yy}, N_{zz})$  denote the total in-plane force resultants,  $(M_{xx}, M_{yy}, M_{zz})$  the moment resultants, and  $(P_{xx}, P_{yy}, P_{zz})$  and  $(R_x, R_y)$  denote the higher-order stress resultants.

The stress resultants  $\{N\}$  and  $\{M\}$  associated with the smart layers are defined by

$$\begin{Bmatrix} N_{xx}^M \\ N_{yy}^M \\ N_{xy}^M \end{Bmatrix} = \sum_{k=1}^N \int_{z_k}^{z_{k+1}} \begin{Bmatrix} \bar{e}_{31} \\ \bar{e}_{32} \\ \bar{e}_{36} \end{Bmatrix}^{(k)} H_z dz, \quad \begin{Bmatrix} M_{xx}^M \\ M_{yy}^M \\ M_{xy}^M \end{Bmatrix} = \sum_{k=1}^N \int_{z_k}^{z_{k+1}} \begin{Bmatrix} \bar{e}_{31} \\ \bar{e}_{32} \\ \bar{e}_{36} \end{Bmatrix}^{(k)} H_z z dz, \quad \begin{Bmatrix} P_{xx}^M \\ P_{yy}^M \\ P_{xy}^M \end{Bmatrix} = \sum_{k=1}^N \int_{z_k}^{z_{k+1}} \begin{Bmatrix} \bar{e}_{31} \\ \bar{e}_{32} \\ \bar{e}_{36} \end{Bmatrix}^{(k)} H_z z^3 dz \quad (5)$$

## 2.5 Velocity feedback control

Considering velocity proportional closed-loop feedback control, the magnetic field intensity  $H$  is expressed in terms of coil constant  $I(x, y, t)$  as

$$H(x, y, t) = k_c I(x, y, t) \quad (6)$$

and  $I(x, y, t)$  is related to the velocity  $w_0$  by

$$I(x, y, t) = c(t) \frac{\partial w_0}{\partial t} \quad (7)$$

where  $k_c$  is the coil constant, which can be expressed in terms of the coil width  $b_c$ , coil radius  $r_c$ , and number of turns  $n_c$  in the coil by

$$k_c = \frac{n_c}{\sqrt{b_c^2 + 4r_c^2}} \quad (8)$$

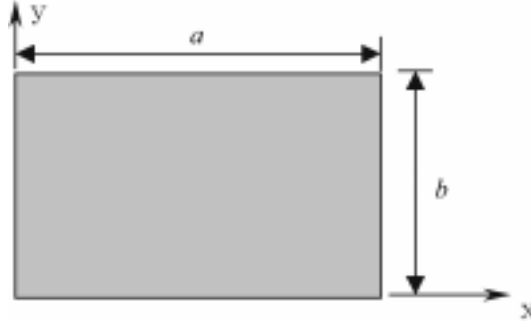


Fig. 2 Geometry and coordinate system used for the Navier solution

and  $c(t)$  is the control gain. In this study the control gain is assumed to be constant. Hence it is represented as  $c$ .

### 3. Analytical Solution

The equations of motion Eq. (3) can be expressed in terms of displacements ( $u_0, v_0, w_0, \varphi_x, \varphi_y$ ) by substituting for the force and moment resultants in terms of the displacements. Due to the assumption of symmetry of the composite laminated plate,  $u_0$  and  $v_0$  are uncoupled from the bending deflections. Hence, it is sufficient to consider only the bending equations. For simply supported rectangular plates, it is possible to obtain the Navier solutions. The simply supported boundary conditions can be expressed as

$$\begin{aligned} \varphi_x(x, 0, t) &= 0, \varphi_x(x, b, t) = 0, \varphi_y(0, y, t) = 0, \varphi_y(a, y, t) = 0, \\ w_0(x, 0, t) &= 0, w_0(x, b, t) = 0, w_0(0, y, t) = 0, w_0(a, y, t) = 0 \\ \bar{M}_{xx}(x, y, t) &= 0, \bar{M}_{xx}(a, y, t) = 0, \bar{M}_{yy}(x, 0, t) = 0, \bar{M}_{yy}(x, b, t) = 0 \end{aligned} \quad (9)$$

The boundary conditions can be satisfied by the following expansions of the displacements:

$$\begin{aligned} w_0(x, y, t) &= \sum_{n=1}^{\infty} \sum_{m=1}^{\infty} W_{mn}(t) \sin \alpha x \sin \beta y \\ \varphi_x(x, y, t) &= \sum_{n=1}^{\infty} \sum_{m=1}^{\infty} X_{mn}(t) \cos \alpha x \sin \beta y \\ \varphi_y(x, y, t) &= \sum_{n=1}^{\infty} \sum_{m=1}^{\infty} Y_{mn}(t) \sin \alpha x \cos \beta y \end{aligned} \quad (10)$$

where  $\alpha = m\pi/a$ ,  $\beta = n\pi/b$ . The coefficients ( $W_{mn}, X_{mn}, Y_{mn}$ ) are unknowns to be determined. The loads are also expanded in double Fourier series

$$\begin{aligned} M_{xx}^M(x, y, t) &= \sum_{n=1}^{\infty} \sum_{m=1}^{\infty} M_{mn}^1(t) \cos \alpha x \sin \beta y \\ M_{xx}^M(x, y, t) &= \sum_{n=1}^{\infty} \sum_{m=1}^{\infty} M_{mn}^2(t) \sin \alpha x \cos \beta y \end{aligned}$$

$$\begin{aligned}
P_{xx}^M(x, y, t) &= \sum_{n=1}^{\infty} \sum_{m=1}^{\infty} P_{mn}^1(t) \cos \alpha x \sin \beta y \\
P_{xx}^M(x, y, t) &= \sum_{n=1}^{\infty} \sum_{m=1}^{\infty} P_{mn}^2(t) \sin \alpha x \cos \beta y
\end{aligned} \tag{11}$$

where, for example, the coefficients are defined by

$$\begin{aligned}
M_{mn}^1(t) &= \frac{4}{ab} \int_0^a \int_0^b M_{xx}^M(x, y, t) \sin \alpha x \sin \beta y dx dy \\
M_{mn}^2(t) &= \frac{4}{ab} \int_0^a \int_0^b M_{yy}^M(x, y, t) \sin \alpha x \sin \beta y dx dy \\
P_{mn}^1(t) &= \frac{4}{ab} \int_0^a \int_0^b P_{yy}^M(x, y, t) \sin \alpha x \sin \beta y dx dy \\
P_{mn}^2(t) &= \frac{4}{ab} \int_0^a \int_0^b P_{yy}^M(x, y, t) \sin \alpha x \sin \beta y dx dy
\end{aligned} \tag{12}$$

Substituting the expansions (12) into the governing equations expressed in terms of the generalized displacements, we obtain

$$\begin{bmatrix} \hat{S}_{33} & \hat{S}_{34} & \hat{S}_{35} \\ \hat{S}_{43} & \hat{S}_{44} & \hat{S}_{45} \\ \hat{S}_{53} & \hat{S}_{54} & \hat{S}_{55} \end{bmatrix} \begin{Bmatrix} W_{mn} \\ X_{mn} \\ Y_{mn} \end{Bmatrix} + \begin{bmatrix} \hat{C}_{33} & 0 & 0 \\ \hat{C}_{43} & 0 & 0 \\ \hat{C}_{53} & 0 & 0 \end{bmatrix} \begin{Bmatrix} \dot{W}_{mn} \\ \dot{X}_{mn} \\ \dot{Y}_{mn} \end{Bmatrix} + \begin{bmatrix} \hat{M}_{33} & \hat{M}_{34} & \hat{M}_{35} \\ \hat{M}_{43} & \hat{M}_{44} & 0 \\ \hat{M}_{53} & 0 & \hat{M}_{55} \end{bmatrix} \begin{Bmatrix} \ddot{W}_{mn} \\ \ddot{X}_{mn} \\ \ddot{Y}_{mn} \end{Bmatrix} = \begin{Bmatrix} Q_{mn} \\ 0 \\ 0 \end{Bmatrix} \tag{13}$$

where  $\hat{S}_{ij}$ ,  $\hat{C}_{ij}$  and  $\hat{M}_{ij}$  are defined by

$$\begin{aligned}
\hat{S}_{33} &= \bar{A}_{55} \alpha^2 + \bar{A}_{44} \beta^2 + c_1^2 [H_{11} \alpha^4 + 2(H_{12} + 2H_{66}) \alpha^2 \beta^2 + H_{22} \beta^4 + \alpha^2 \beta^2 + H_{22} \beta^4] \\
\hat{S}_{34} &= \bar{A}_{55} \alpha - c_1 [\hat{F}_{11} \alpha^3 + (\hat{F}_{12} + 2\hat{F}_{66}) \alpha \beta^2] \\
\hat{S}_{35} &= \bar{A}_{44} \beta - c_1 [\hat{F}_{22} \beta^3 + (\hat{F}_{12} + 2\hat{F}_{66}) \alpha^2 \beta] \\
\hat{C}_{34} &= \hat{C}_{35} = 0 \\
\hat{C}_{33} &= \in_{31} (\alpha^2 + \beta^2) \\
\hat{M}_{33} &= I_0 + c_1^2 I_6 (\alpha^2 + \beta^2), \quad \hat{M}_{34} = -c_1 J_4 \alpha = \hat{M}_{43}, \quad \hat{M}_{35} = -c_1 J_4 \beta \\
\hat{S}_{43} &= \bar{A}_{55} \alpha - c_1 [\hat{F}_{11} \alpha^3 + (\hat{F}_{12} + 2\hat{F}_{66}) \alpha \beta^2] \\
\hat{S}_{44} &= \bar{A}_{55} + \bar{D}_{11} \alpha^2 + \bar{D}_{66} \beta^2 \\
\hat{S}_{45} &= (\bar{D}_{12} + \bar{D}_{66}) \alpha \beta \\
\hat{C}_{43} &= \alpha \in_{32} \\
\hat{C}_{44} &= \hat{C}_{45} = 0 \\
\hat{M}_{44} &= K_2, \quad \hat{M}_{45} = 0, \quad \hat{M}_{55} = K_2 \\
\in_{31} &= -c_1 \tilde{p} k_c c, \quad \in_{32} = -(\tilde{m} - c_1 \tilde{p}) k_c c
\end{aligned}$$

$$\begin{aligned}
\hat{S}_{53} &= \bar{A}_{44}\beta - c_1 [\hat{F}_{22}\beta^3 + (\hat{F}_{12} + 2\hat{F}_{66})\alpha^2\beta] \\
\hat{S}_{54} &= (\bar{D}_{12} + \bar{D}_{66})\alpha\beta \\
\hat{S}_{55} &= \bar{A}_{44} + \bar{D}_{66}\alpha^2 + \bar{D}_{22}\beta^2 \\
\hat{C}_{53} &= \beta \in_{33}, \quad \in_{33} = -(\tilde{m} - c_1 \tilde{p})k_c c \\
\hat{C}_{54} &= \hat{C}_{55} = 0 \\
\hat{M}_{53} &= -c_1 J_4 \beta, \quad \hat{M}_{55} = K_2 \\
\tilde{p} &= \int \bar{e}_{31} z^3 dz
\end{aligned} \tag{14}$$

For vibration control, the solution of the ordinary differential equations in Eq. (13) are obtained in the form

$$W_{mn}(t) = W_0 e^{\lambda t}, \quad X_{mn}(t) = X_0 e^{\lambda t}, \quad Y_{mn}(t) = Y_0 e^{\lambda t} \tag{15}$$

and obtain, for non-trivial solution, the result

$$\begin{vmatrix} \bar{S}_{33} & \bar{S}_{34} & \bar{S}_{35} \\ \bar{S}_{43} & \bar{S}_{44} & \bar{S}_{45} \\ \bar{S}_{53} & \bar{S}_{54} & \bar{S}_{55} \end{vmatrix} = 0 \tag{16}$$

where

$$\bar{S}_{ij} = \hat{S}_{ij} + \lambda \hat{C}_{ij} + \lambda^2 \hat{M}_{ij} \tag{17}$$

for  $i, j=3, 4, 5$ . This equation gives three sets of eigenvalues. The lowest one corresponds to the transverse motion. The eigenvalues can be written as  $\lambda = -\alpha_d + i\omega_d$ , so that the damped motion is given by

$$w_0(x, y, t) = \frac{1}{\omega_d} e^{-\alpha_d t} \sin \omega_d t \sin \frac{m\pi x}{a} \sin \frac{n\pi y}{b} \tag{18}$$

In arriving at the last solution, the following initial conditions are used:

$$\begin{aligned}
w_0(x, y, 0) &= 0, \quad \dot{w}_0(x, y, 0) = 1, \quad \varphi_x(x, y, 0) = 0 \\
\varphi_y(x, y, 0) &= 0, \quad \dot{\varphi}_x(x, y, 0) = 0, \quad \dot{\varphi}_y(x, y, 0) = 0
\end{aligned} \tag{19}$$

#### 4. Finite element model

The nodal variables of the third-order theory are  $(w_0, w_{0,n} = \partial w_0 / \partial n, \varphi_n, \varphi_s)$ , where  $(\varphi_n, \varphi_s)$  are the rotations of a transverse line about the in-plane normal and tangent. Lagrange interpolation functions of  $(\varphi_n, \varphi_s)$  and Hermite interpolation function for  $w_0$  are used for the formulation of the displacement finite element model. A conforming element that has eight degrees of freedom  $(w_0, w_{0,x}, w_{0,y}, w_{0,xy}, \varphi_x, \varphi_y)$  is used (Reddy 1997).

The generalized displacements are approximated over an element  $\Omega^e$  by the expressions

$$\begin{aligned}
w_0(x,y,t) &= \sum_{i=1}^m \bar{\Delta}_i^e(t) \phi_i^e(x,y) \\
\varphi_x(x,y,t) &= \sum_{i=1}^m X_i^e(t) \psi_i^e(x,y) \\
\varphi_y(x,y,t) &= \sum_{i=1}^m Y_i^e(t) \psi_i^e(x,y)
\end{aligned} \tag{20}$$

where  $\psi_i^e$  denote the Lagrange interpolation functions and  $\phi_i^e$  are the Hermite interpolation functions. The four nodal values associated with  $w_0$  are

$$\bar{\Delta}_1 = w_0, \bar{\Delta}_2 = \frac{\partial w_0}{\partial x}, \bar{\Delta}_3 = \frac{\partial w_0}{\partial y}, \bar{\Delta}_4 = \frac{\partial^2 w_0}{\partial x \partial y} \tag{21}$$

The finite element model is of the form

$$\begin{aligned}
& \begin{bmatrix} [K^{11}] & [K^{12}] & [K^{13}] & [K^{14}] & [K^{15}] \\ [K^{12}]^T & [K^{22}] & [K^{23}] & [K^{24}] & [K^{25}] \\ [K^{13}]^T & [K^{32}]^T & [K^{33}] & [K^{34}] & [K^{35}] \\ [K^{14}]^T & [K^{24}]^T & [K^{34}]^T & [K^{44}] & [K^{45}] \\ [K^{15}]^T & [K^{25}]^T & [K^{53}]^T & [K^{45}]^T & [K^{55}] \end{bmatrix} \begin{Bmatrix} \{u^e\} \\ \{v^e\} \\ \{\bar{\Delta}^e\} \\ \{X^e\} \\ \{Y^e\} \end{Bmatrix} + \\
& \begin{bmatrix} [C^{11}] & [C^{12}] & [C^{13}] & [C^{14}] & [C^{15}] \\ [C^{21}]^T & [C^{22}] & [C^{23}] & [C^{24}] & [C^{25}] \\ [C^{13}]^T & [C^{23}]^T & [C^{33}] & [C^{34}] & [C^{35}] \\ [C^{14}]^T & [C^{24}]^T & [C^{43}] & [C^{44}] & [C^{45}] \\ [C^{15}]^T & [C^{25}]^T & [C^{53}] & [C^{45}]^T & [C^{55}] \end{bmatrix} \begin{Bmatrix} \{u^e\} \\ \{v^e\} \\ \{\bar{\Delta}^e\} \\ \{X^e\} \\ \{Y^e\} \end{Bmatrix} + \\
& \begin{bmatrix} [M^{11}] & [0] & [M^{13}] & [M^{14}] & [0] \\ [0]^T & [M^{22}] & [M^{23}] & [0] & [M^{25}] \\ [M^{13}]^T & [M^{23}]^T & [M^{33}] & [M^{34}] & [M^{35}] \\ [M^{14}]^T & [0]^T & [M^{34}]^T & [M^{44}] & [0] \\ [0]^T & [M^{25}]^T & [M^{53}]^T & [0]^T & [M^{55}] \end{bmatrix} \begin{Bmatrix} \{u^e\} \\ \{v^e\} \\ \{\bar{\Delta}^e\} \\ \{X^e\} \\ \{Y^e\} \end{Bmatrix} = 0
\end{aligned} \tag{22}$$

or in compact form

$$\sum_{\beta=1}^5 \sum_{j=1}^{n_\beta} (K_{ij}^{\alpha\beta} \Delta_j^\beta + C_{ij}^{\alpha\beta} \dot{\Delta}_j^\beta + M_{ij}^{\alpha\beta} \ddot{\Delta}_j^\beta) - F_i^\alpha = 0, i=1, 2, \dots, n \tag{23}$$

where  $\alpha=1, 2, 3, 4, 5$ ;  $n_1=n_2=n_4=n_5=4$  and  $n_3=16$ . The nodal values  $\Delta_j^\beta$  are

$$\Delta_j^1 = u_j, \Delta_j^2 = v_j, \Delta_j^3 = \bar{\Delta}_j, \Delta_j^4 = X_j^1, \Delta_j^5 = Y_j^2$$

For the details of the finite element coefficient matrices see Reddy (1997, 1999a).

## 5. Results and discussion

### 5.1 Introduction

The reason for using magnetostrictive material in this work is to satisfy the requirement of smart material actuators to have high energy density, negligible weight, and point excitation with a wide frequency bandwidth. A typical magnetostrictive actuator consists of two identical magnetostrictive rods held between two end plates made of magnetic material (Ni-Fe) alloy. The surrounding magnetic coils drive each Terfenol-D rod separately. The rods can be pre-stressed using Belleville disk springs and a screw located between the two rods. The Belleville disk springs are non-linear in nature providing a deflection range over which the preload is maintained constant. The two end plates serve two purposes: they provide (1) a means to preload the rods and (2) a least resistance path for the magnetic flux generated by the coils. The coils are so energized that the magnetic flux generated by them add up to make the actuator most efficient. By this method both the forward and return flux paths will be performing useful work. Terfenol-D has the characteristics of being able to produce strains up to 2500  $\mu\text{m}$ , which is of an order of magnitude superior to the current generation of piezoceramic materials, and also has an energy density as high as 25000  $\text{Jm}^{-3}$ . The material properties of Terfenol-D are listed in Table 1.

Four different kinds of the elastic composite materials are used. CFRP [composite fiber reinforced polymer], Gr-Ep (AS) [graphite-epoxy], Gl-Ep [glass epoxy], Br-Ep [boron epoxy]. The structural properties of these materials are listed in Table 2.

### 5.2 Numerical solutions

Using the analytical solutions and finite element models developed in Sections 3 and 4, numerical studies are carried out. In particular, the following parametric studies were carried out to determine the effect on the frequency and vibration suppression time:

- (1) The effect of the position of the smart material layer.
- (2) The thickness of the smart material layer and the elastic composite layer.
- (3) The material properties of the elastic layer.

Table 1 Terfenol-D material properties

$E_m$ [GPa]	$\rho_m$ [ $\text{Kg m}^{-3}$ ]	$D_k$ [ $10^{-8} \text{ mA}^{-1}$ ]	$\nu_m$
26.5	9250	1.67	0

Table 2 Engineering material properties of various composite materials

Material	$E_1$ [Gpa]	$E_2$ [GPa]	$G_{13}$ [GPa]	$G_{23}$ [GPa]	$G_{12}$ [GPa]	$\nu_{12}$	$\rho$ [ $\text{Kg m}^{-3}$ ]
CFRP	138.6	8.27	4.96	4.96	4.12	0.26	1824
Gr-Ep(AS)	137.9	8.96	7.20	6.21	7.20	0.30	1450
Gl-Ep	53.78	17.93	8.96	3.45	8.96	0.56	1900
Br-Ep	206.9	20.69	6.9	4.14	6.9	0.30	1950

The vibration suppression time is defined as the time required to reduce the uncontrolled vibration amplitude to one-tenth of its initial amplitude. Various values of the vibration suppression time ratio  $T_s$  (suppression time divided by the maximum suppression time) are obtained as the distance between the magnetostrictive layers and the neutral axis is varied. The vibration suppression time ratio can be shown to be  $T_s = h_m / 2z_m$ , where  $h_m$  is the thickness of the magnetostrictive layer and  $z_m$  is the distance between the mid-plane of the magnetostrictive layer and the mid plane of the plate. Studies involving different lamination schemes, layer thickness, and control gain values have also been carried out.

To obtain the frequencies and the damping parameter, Eq. (23) should be solved. Eq. (23) can be expressed as

$$[S]\{U\} + [C]\{\dot{U}\} + [M]\{\ddot{U}\} = 0 \tag{27}$$

which can be rewritten as

$$\begin{bmatrix} 0 & [M] \\ [M] & [C] \end{bmatrix} \begin{bmatrix} \{\ddot{U}\} \\ \{\dot{U}\} \end{bmatrix} + \begin{bmatrix} -[M] & 0 \\ 0 & [S] \end{bmatrix} \begin{bmatrix} \{\dot{U}\} \\ \{U\} \end{bmatrix} = \{0\} \tag{28}$$

or  $[A]\{\dot{Y}\} + [B]\{Y\} = 0$  where  $\begin{bmatrix} \{\dot{U}\} \\ \{U\} \end{bmatrix} = \{Y\}$ . This system is then solved using *Mathcad*, a mathematical software tool to obtain the eigenvalues, which are then used to determine the solution (18).

### 5.3 Effect of lamina material properties

The influence of lamina material properties on the amplitude of vibration and vibration suppression times has been studied and the results are tabulated. Table 3 lists the inertial coefficients of the different lamination schemes used. The lamination scheme used in all the materials is  $[\pm 45/\mathbf{m}/0/90]_s$ . This lamination scheme means that the laminated plate consists of 10 laminae, the fiber orientation being  $[+45/-45/\mathbf{m}/0/90/90/0/\mathbf{m}/-45/45]$ . Here  $\mathbf{m}$  stands for the magnetostrictive material layer and the subscript “S” stands for symmetric.

Table 4 contains the frequencies  $\omega_d$  and damping coefficient  $\alpha_d$  obtained using different composite materials. Fig. 3 shows the plots of vibration suppression characteristics of composite plates made up of different materials. It is observed that materials having almost same  $E_1/E_2$  ratios have similar

Table 3 Inertial coefficients of different lamination schemes

Material	Laminate	$I_0$ [kg m <sup>-2</sup> ]	$I_2$ (10 <sup>-4</sup> ) [kg m <sup>-1</sup> ]	$I_4$ (10 <sup>-9</sup> ) [kg m <sup>3</sup> ]	$I_6$ (10 <sup>-14</sup> ) [kg m <sup>5</sup> ]
CFRP	$[\pm 45/\mathbf{m}/0/90]_s$	33.09	2.461	2.907	4.508
	$[45/\mathbf{m}/-45/0/90]_s$	33.09	3.352	4.600	7.084
	$[\mathbf{m}/\pm 45/0/90]_s$	33.09	4.54	8.521	17.171
	$[\mathbf{m}/90_4]_s$	33.09	4.54	8.521	17.171
	$[\mathbf{m}/0_4]_s$	33.09	4.54	8.521	17.171
Gr-Ep(AS)	$[\pm 45/\mathbf{m}/0/90]_s$	30.1	2.196	2.471	3.696
Gl-Ep	$[\pm 45/\mathbf{m}/0/90]_s$	33.7	2.514	2.995	4.674
Br-Ep	$[\pm 45/\mathbf{m}/0/90]_s$	34.1	2.55	3.054	4.782

Table 4 Damping coefficients and frequencies for different materials ( $h_e=1$  mm,  $h_m=1$  mm)

Material	Laminate	$-\alpha_d \pm \omega_d$ [rad s <sup>-1</sup> ]
CFRP	$[\pm 45/\mathbf{m}/0/90]_s$	$6.543 \pm 254.791$
Gr-Ep(AS)	$[\pm 45/\mathbf{m}/0/90]_s$	$7.242 \pm 264.513$
Gl-Ep	$[\pm 45/\mathbf{m}/0/90]_s$	$6.475 \pm 187.462$
Br-Ep	$[\pm 45/\mathbf{m}/0/90]_s$	$6.320 \pm 309.998$

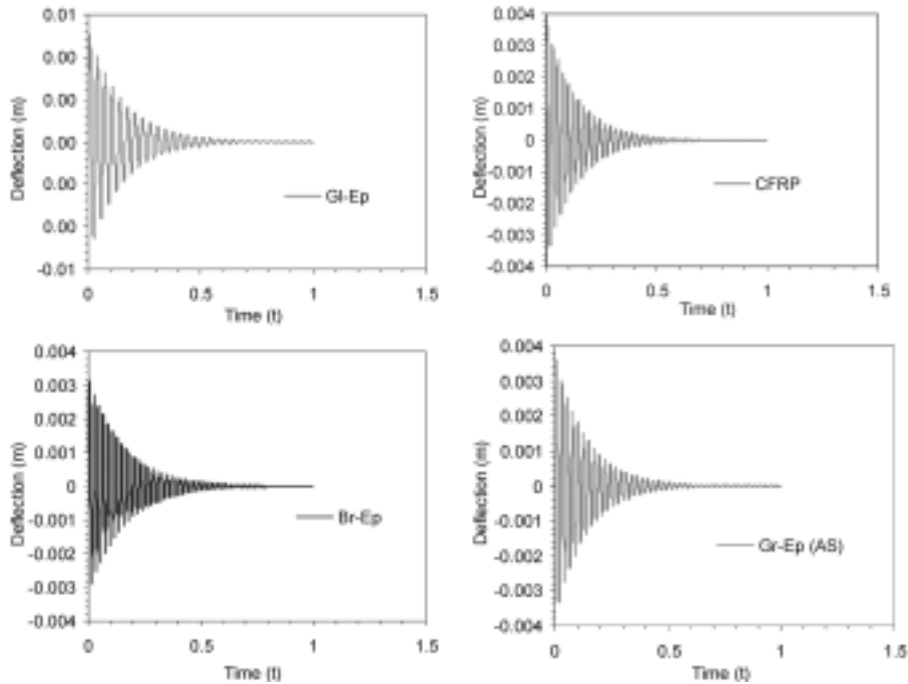


Fig. 3 Effect of material properties on vibration suppression

vibration suppression characteristics.

Since the classical laminate plate theory (CLPT) and the first-order shear deformation theory (FSDT) are mere special cases of the third-order shear deformation theory (TSDT), it is possible to obtain solutions of the CLPT and FSDT as special cases from the formulations presented herein. A comparison of the eigenvalues obtained using the three theories is presented in Table 5. It is observed that the CLPT gives higher frequencies of vibration. This is expected, as the CLPT theory renders the plate stiffer compared to the other two theories.

#### 5.4 Effect of the position of the smart material layer

The suppression times for a CFRP laminate are studied and the results are presented in Table 6. The thickness of the lamina  $h_e$  is taken to be 5 mm and the thickness of the smart material layer  $h_m$  is taken to be 2 mm. The natural frequencies and the damping coefficients for different lamination schemes are obtained. The maximum deflections  $W_{\max}$  of the composite plate and the suppression

Table 5 Comparison of the eigenvalues obtained through CLPT, FSDT, and TSDT ( $h_e=1$  mm, and  $h_m=1$  mm)

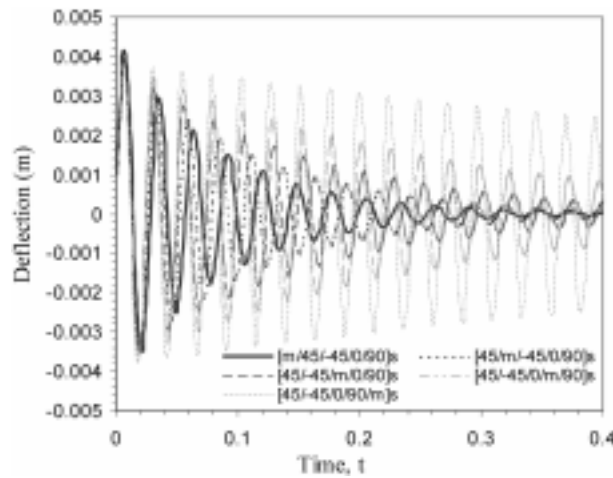
Material	Laminate	$-\alpha_d \pm \omega_d$ [rad s <sup>-1</sup> ] CLPT	$-\alpha_d \pm \omega_d$ [rad s <sup>-1</sup> ] FSDT	$-\alpha_d \pm \omega_d$ [rad s <sup>-1</sup> ] TSDT
CFRP	[±45/0/90/ <b>m</b> ] <sub>s</sub>	1.318 ± 259.311	1.317 ± 259.160	1.372 ± 258.812
	[±45/0/ <b>m</b> /90] <sub>s</sub>	3.956 ± 258.482	3.952 ± 257.723	3.983 ± 257.157
	[±45/ <b>m</b> /0/90] <sub>s</sub>	6.591 ± 255.376	6.587 ± 254.823	6.543 ± 254.791
	[45/ <b>m</b> /-45/0/90] <sub>s</sub>	9.231 ± 241.059	9.224 ± 240.724	9.402 ± 240.543
	[ <b>m</b> /±45/0/90] <sub>s</sub>	11.865 ± 221.872	11.861 ± 221.418	11.981 ± 221.275

Table 6 Suppression time ratio for different CFRP laminates ( $h_e=5$  mm and  $h_m=2$  mm)

Laminates	$z_m$ (m)	$-\alpha_d$	$\pm \omega_d$	$W_{\max}$ (10 <sup>-3</sup> m)	$t$ at $W_{\max}/10$	$T_s$
[±45/0/90/ <b>m</b> ] <sub>s</sub>	0.001	1.531	1286.781	0.7689	1.4350	1.0000
[±45/0/ <b>m</b> /90] <sub>s</sub>	0.006	12.261	1085.873	0.8213	0.2411	0.1660
[±45/ <b>m</b> /0/90] <sub>s</sub>	0.011	25.983	1072.518	0.8024	0.1309	0.0909
[45/ <b>m</b> /-45/0/90] <sub>s</sub>	0.016	39.719	1006.792	0.8298	0.0898	0.0625
[ <b>m</b> /±45/0/90] <sub>s</sub>	0.021	53.650	905.857	0.9673	0.0685	0.0476

times have been calculated. Here  $z_m$  denotes the positive distance from the center of the laminate to the center of the smart layer.

Fig. 4 shows the plots of fundamental mode of vibration versus time for various laminates. It is observed that as the smart material layer is moved farther from the mid-plane the suppression time decreases. This is due to the fact that the moment applied by the actuation of the smart material on the structure is more as the smart material is moved away from the mid-plane. Fig. 5 shows the effect of moving the smart material layer away from the mid-plane on the vibration suppression time. It is observed that the vibration suppression time does not show appreciable change when the distance of the smart material layer from the mid-plane is reduced from 0.021 m to 0.011 m, but

Fig. 4 Vibration suppression characteristics for different CFRP laminates ( $h_e=5$  mm,  $h_m=2$  mm)

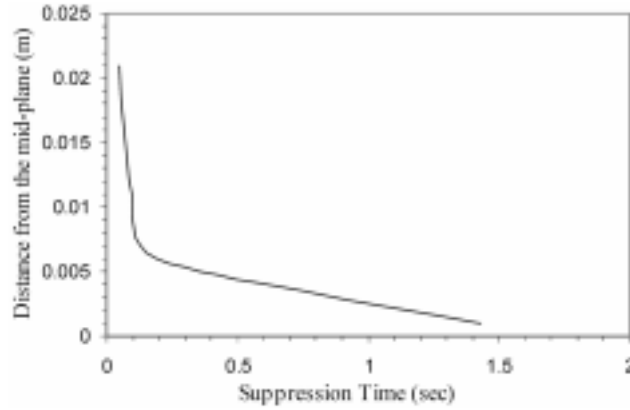


Fig. 5 Vibration suppression times for CFRP laminates ( $h_e=5$  mm,  $h_m=2$  mm)

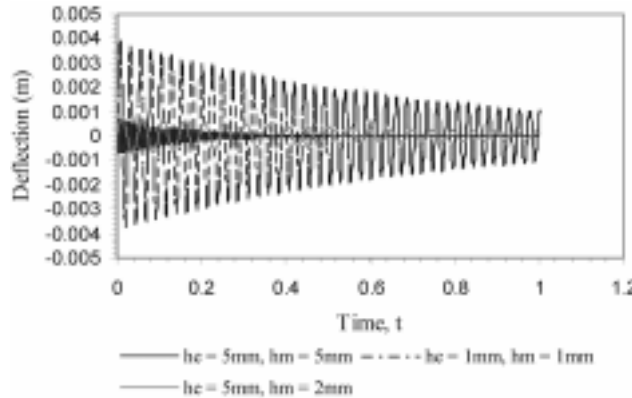


Fig. 6 Effect of lamina thickness on vibration suppression

then increases by almost an order of magnitude when the smart material layer is moved from 0.011 m to 0.001 m from the mid-plane. This is due to the non-linearity caused by the  $z_m$  term in the definition of  $T_s$ .

### 5.5 Effect of the lamina thickness

The vibration characteristics are obtained for the CFRP laminate with the fiber orientation of  $[\pm 45/0/90/\mathbf{m}]_s$  for different thicknesses of the lamina and smart material layers, while keeping the control gain constant. The vibration frequencies, damping factors, suppression times, and the suppression time ratios are presented in Table 7 for ( $h_e=1$  mm,  $h_m=1$  mm), ( $h_e=5$  mm,  $h_m=2$  mm), and ( $h_e=5$  mm,  $h_m=5$  mm). Also, see Fig. 6.

### 5.6 Effect of the feedback coefficient on suppression time

The value of the feedback coefficient  $c(t)k_c$  influences the vibration suppression characteristics. The study is performed on a CFRP laminate with thickness of the elastic layer to be 5 mm and the

Table 7 Vibration suppression characteristics for CFRP laminate of orientation  $[\pm 45/0/90/m]_s$

Thickness (mm)	$-\alpha_d$	$\pm\omega_d$ (rad s <sup>-1</sup> )	$W_{\max}$ (10 <sup>-3</sup> m)	$t$ (sec) at $W_{\max}/10$
$h_e=1, h_m=1$	1.372	258.812	3.8710	1.7720
$h_e=5, h_m=2$	1.531	1286.781	0.7689	1.4350
$h_e=5, h_m=5$	6.322	1252.58	0.7581	0.3702

thickness of the smart material to be 5 mm. Different lamination schemes are used and the position of the smart material layer is varied. Two different values of the feedback coefficient are used:  $c(t)k_c=10^4$  and  $c(t)k_c=10^3$ .

Plots of the variation of the vibration suppression time for different laminates and for two

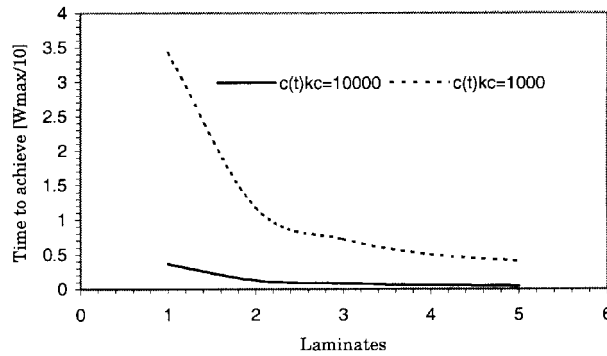


Fig. 7 Effect of feedback coefficient on the suppression time. (1)  $[\pm 45/0/90/m]_s$ , (2)  $[\pm 45/0/m/90]_s$ , (3)  $[\pm 45/m/0/90]_s$ , (4)  $[45/m/-45/0/90]_s$ , (5)  $[m/\pm 45/0/90]_s$

Table 8 Suppression time ratio for two control gains for different CFRP laminates ( $h_e=5$  mm and  $h_m=5$  mm)

a)

Laminate	$z_m$ (m)	$c(t)k_c=10^4$				
		$-\alpha_d$	$\pm\omega_d$	$W_{\max}$	$t$	$T_s$
$[\pm 45/0/90/m]_s$	0.0025	6.322	1252.58	0.7581	0.3702	1.000
$[\pm 45/0/m/90]_s$	0.0075	18.983	1245.15	0.7493	0.1241	0.3333
$[\pm 45/m/0/90]_s$	0.0125	31.672	1230.98	0.7435	0.0752	0.200
$[45/m/45/0/90]_s$	0.0175	44.514	1165.12	0.7549	0.0530	0.1429
$[m/\pm 45/0/90]_s$	0.0225	57.751	1071.83	0.7744	0.0418	0.1111

b)

Laminate	$z_m$ (m)	$c(t)k_c=10^3$				
		$-\alpha_d$	$\pm\omega_d$	$W_{\max}$	$t$	$T_s$
$[\pm 45/0/90/m]_s$	0.0025	0.632	1252.64	0.7612	3.5132	1.000
$[\pm 45/0/m/90]_s$	0.0075	1.894	1245.21	0.7604	1.1779	0.3333
$[\pm 45/m/0/90]_s$	0.0125	3.173	1231.05	0.7682	0.7109	0.200
$[45/m/45/0/90]_s$	0.0175	4.450	1165.24	0.8112	0.5031	0.1429
$[m/\pm 45/0/90]_s$	0.0225	5.774	1070.97	0.8524	0.3969	0.1111

different values of the feedback control coefficient are presented in Fig. 7. It can be seen that the suppression time increases when the value of the feedback coefficient decreases. This is expected because the coefficients of the damping matrix decrease, thereby resulting in less damping. However, from Table 8, it can be noted that there is no appreciable change in the natural frequency of vibration for different lamination schemes when the value of the feedback coefficient changes.

### 5.7 Effect of lamination scheme

The vibration suppression characteristics are studied for a number of lamination schemes. In addition to the lamination schemes and different thickness of the elastic lamina and the smart material lamina used earlier, composite plates with more number of layers and fiber orientations are examined for vibration suppression. These results have been tabulated in Tables 9 and 10. Here again the analysis has been done for different positions of the smart material layer, and the effect of smart material layer position on the vibration suppression time is studied.

### 5.8 Variation of $T_s$ and $\epsilon_{31}$ for different laminates

The variation of the vibration suppression ratio  $T_s$  and the normalized damping parameter  $e_r = (\epsilon_{31}/\epsilon_{\max})$  is studied for different positions of the smart material layer in the composite laminated plate. The results are tabulated in Table 11, and plots are presented in Fig. 8. From the earlier

Table 9 Suppression time ratio for different CFRP laminates ( $h_e=3$  mm and  $h_m=3$  mm)

Laminates	$z_m$ (m)	$-\alpha_d$	$\pm\omega_d$	$W_{\max}$ ( $10^{-3}$ m)	$t$ at $W_{\max}/10$ (sec)	$T_s$
$[\pm 45/0/90/\pm 30/60/\mathbf{m}]_S$	0.0015	3.423	1406.03	0.7090	0.6370	1.0000
$[\pm 45/0/90/\pm 30/\mathbf{m}/60]_S$	0.0045	8.541	1279.65	0.7461	0.2134	0.3333
$[\pm 45/0/90/30/\mathbf{m}/-30/60]_S$	0.0075	14.278	1270.21	0.7459	0.1287	0.2000
$[\pm 45/0/90/\mathbf{m}/\pm 30/60]_S$	0.0105	19.871	1256.32	0.7463	0.0912	0.1428
$[\pm 45/0/\mathbf{m}/90/\pm 30/60]_S$	0.0135	25.728	1248.69	0.7437	0.0721	0.1111
$[\pm 45/\mathbf{m}/0/90/\pm 30/60]_S$	0.0165	31.432	1238.85	0.7422	0.0580	0.0909
$[45/\mathbf{m}/-45/0/90/\pm 30/60]_S$	0.0195	37.194	1203.91	0.7508	0.0491	0.0769
$[\mathbf{m}/\pm 45/0/90/\pm 30/60]_S$	0.0225	42.873	1162.04	0.7611	0.0437	0.0666

Table 10 Suppression time ratio for different CFRP laminates ( $h_e=2.5$  mm and  $h_m=2.5$  mm)

Laminates	$z_m$ (m)	$-\alpha_d$	$\pm\omega_d$	$W_{\max}$ ( $10^{-3}$ m)	$t$ at $W_{\max}/10$ (sec)	$T_s$
$[\pm 5/\pm 60/0/90/\pm 45/30/\mathbf{m}]_S$	0.00125	2.822	1671.43	0.5992	0.7140	1.0000
$[\pm 45/\pm 60/0/90/\pm 45/\mathbf{m}/30]_S$	0.00375	8.441	1671.45	0.5932	0.2535	0.3333
$[\pm 45/\pm 60/0/90/45/\mathbf{m}/-45/30]_S$	0.00625	6.487	1121.87	0.8557	0.1933	0.2000
$[\pm 45/\pm 60/0/90/\mathbf{m}/\pm 45/30]_S$	0.00875	14.114	1397.06	0.7016	0.1494	0.1433
$[\pm 45/\pm 60/0/\mathbf{m}/90/\pm 45/30]_S$	0.01125	18.219	1393.13	0.7015	0.1275	0.1111
$[\pm 45/\pm 60/\mathbf{m}/0/90/\pm 45/30]_S$	0.01375	22.288	1388.02	0.6998	0.1052	0.0909
$[\pm 45/60/\mathbf{m}/-60/0/90/\pm 45/30]_S$	0.01625	26.306	1373.02	0.7011	0.0881	0.0769
$[\pm 45/\mathbf{m}/\pm 60/0/90/\pm 45/30]_S$	0.01875	30.441	1355.09	0.7047	0.0814	0.0666
$[45/\mathbf{m}/-45/\pm 60/0/90/\pm 45/30]_S$	0.02125	34.521	1330.32	0.7112	0.0713	0.0588
$[\mathbf{m}/\pm 45/\pm 60/0/90/\pm 45/30]_S$	0.02375	38.627	1301.37	0.7158	0.0685	0.0526

Table 11 Suppression time ratio and  $\epsilon_{31}$  parameter for different CFRP laminates ( $h_e=1$  mm,  $h_m=1$  mm)

Laminate	$z_m$ (m)	$-\alpha_d$	$\pm\omega_d$	$W_{max}$ ( $10^{-3}$ m)	$t$ (sec) at $W_{max}/10$	$T_s$	$-\epsilon_{31}$	$\frac{E_r}{-\epsilon_{31}/\epsilon_{max}}$
$[\pm 45/0/90/m]_s$	0.0005	1.372	258.812	3.871	1.772	1.000	4.425	0.111
$[\pm 45/0/m/90]_s$	0.0015	3.983	257.157	3.795	0.594	0.333	13.285	0.334
$[\pm 45/m/0/90]_s$	0.0025	6.543	254.791	3.801	0.358	0.200	22.131	0.556
$[45/m/-45/0/90]_s$	0.0035	9.402	240.543	3.904	0.257	0.143	30.982	0.778
$[m/\pm 45/0/90]_s$	0.0045	11.981	221.275	4.162	0.200	0.111	39.833	1.000

discussions, the vibration suppression ratio decreases when the smart material is moved away from the laminate. The normalized damping parameter increases as the smart material layer is moved away from the neutral axis. This is explained by the increased damping that is achieved when the smart material layer is moved away from the neutral axis. The variation is studied on a CFRP laminate with the thickness of the elastic composite layer and the thickness of the smart material layer being 1 mm.

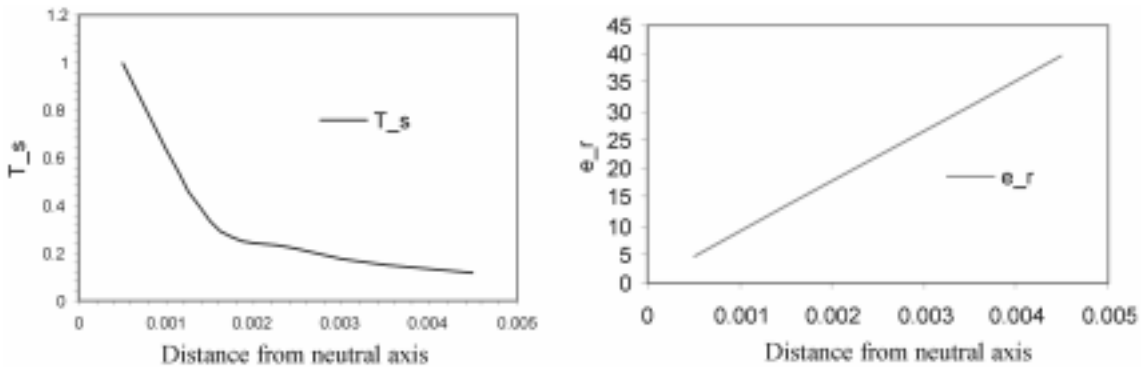


Fig. 8 Variation of  $T_s$  and  $\epsilon_{31}$  with the position of the smart material layer

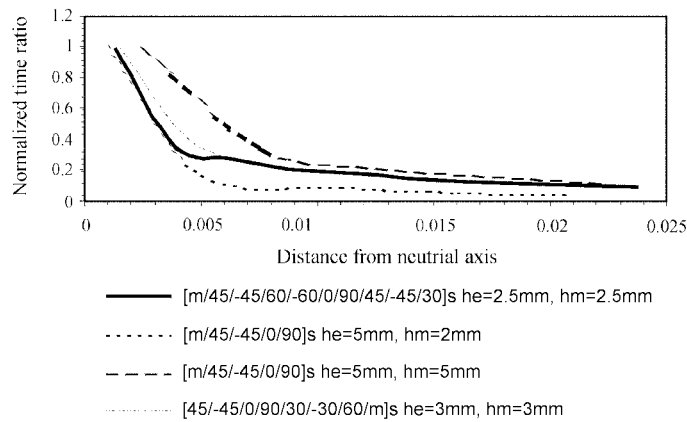


Fig. 9 Variation of time ratio with respect to distance from the neutral axis

### 5.9 Effect of smart material layer position and the thickness of structural layers

Fig. 9 shows the effect of the position and thickness of the smart material layer and the thickness of the composite material layers on the vibration suppression time ratio. From the figure it is observed that thinner smart material layers result in better attenuation of the vibration. This is due to a higher mass matrix that is caused by the large increase in the moment of inertia of the system when thickness of the smart material layer is increased. This increase is because the smart material layer has a density of almost five times to that of the composite material.

### 5.10 Vibration suppression of different modes

The vibration suppression characteristics of the first five vibration modes of the composite plates are also studied. Plots of deflection versus time are presented in Fig. 10.

From the plots it can be seen that the vibration suppression time decreases very rapidly as mode number increases. This is because the amplitude of vibration that has to be suppressed decreases as

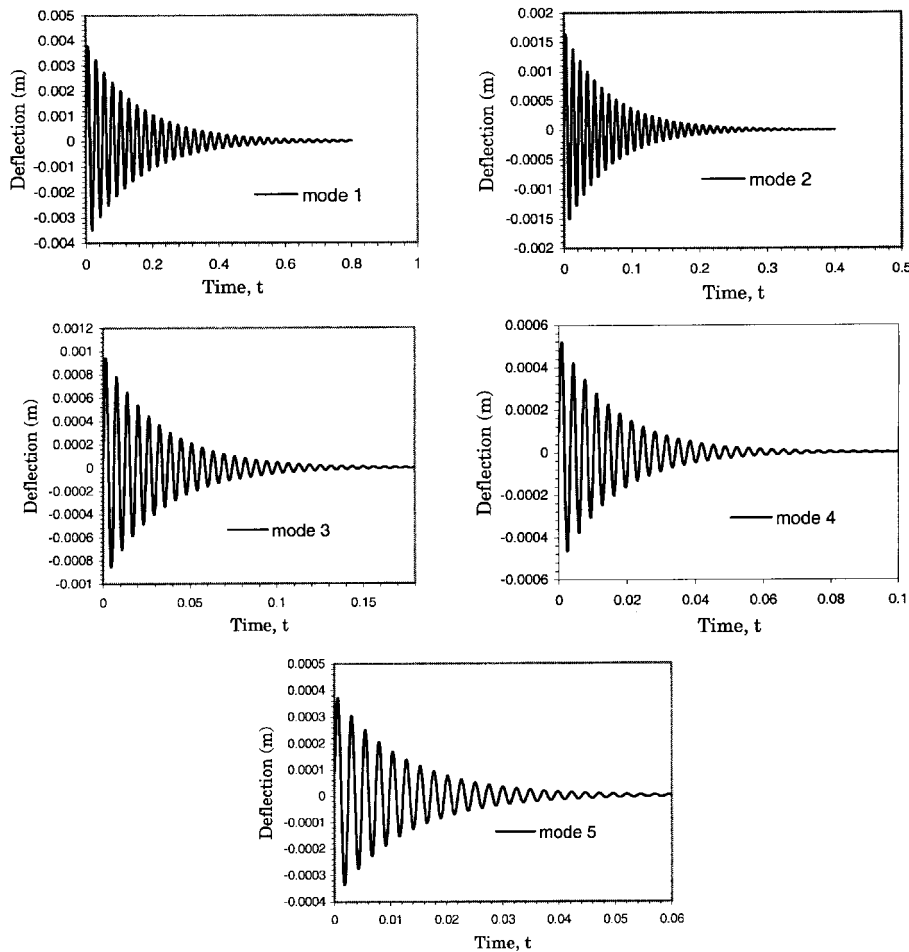


Fig. 10 Suppression characteristics for different modes of vibration

Table 12 Comparison of finite element with analytical results for a CFRP laminate ( $h_e=5$  mm,  $h_m=5$  mm)

Laminate	$z_m$ (m)	Analytical	FEM [4×4]	FEM [2×2]
		$-\alpha_d \pm \omega_d$	$-\alpha_d \pm \omega_d$	$-\alpha_d \pm \omega_d$
[±45/0/90/m] <sub>s</sub>	0.0025	6.322 ± 1252.58	6.287 ± 1252.19	6.203 ± 1251.87
[±45/0/m/90] <sub>s</sub>	0.0075	18.983 ± 1245.15	18.915 ± 1244.75	18.884 ± 1244.43
[±45/m/0/90] <sub>s</sub>	0.0125	31.672 ± 1230.98	31.618 ± 1230.32	31.492 ± 1229.81
[45/m/-45/0/90] <sub>s</sub>	0.0175	44.514 ± 1165.12	44.485 ± 1164.73	44.231 ± 1164.15
[m/±45/0/90] <sub>s</sub>	0.0225	57.751 ± 1071.83	57.697 ± 1071.27	56.983 ± 1070.65

Table 13 Vibration suppression characteristic for a fully clamped CFRP laminated plate  $h_e=5$  mm,  $h_m=5$  mm

Laminates	$z_m$ (m)	$-\alpha_d$	$\pm \omega_d$	$W_{\max}^{\max}$ ( $10^{-3}$ m)	$t$ at $W_{\max}/10$ (sec)	$T_s$
[±45/0/90/m] <sub>s</sub>	0.0025	7.53	1898.61	0.4797	0.3419	1.000
[±45/0/m/90] <sub>s</sub>	0.0075	20.85	1873.35	0.4739	0.1146	0.333
[±45/m/0/90] <sub>s</sub>	0.0125	35.07	1855.91	0.4701	0.0691	0.20
[45/m/-45/0/90] <sub>s</sub>	0.0175	47.88	1814.04	0.4885	0.0489	0.1429
[m/±45/0/90] <sub>s</sub>	0.0225	60.15	1765.29	0.5090	0.0387	0.111

the mode number increases. The results have been obtained for a CFRP [±45/m/0/90]<sub>s</sub> composite laminate with  $h_e=1$  mm and  $h_m=1$  mm. Of course, similar trend should hold for other laminates. Here the value of  $m = 1$ , and  $n$  takes the values 1, 2, 3, 4, 5.

### 5.11 Finite element results

Here the finite element developed herein is validated by comparing with the analytical solution, and then results are obtained for a clamped laminate, for which no analytical solution is available. The element used in the analysis is a 8-noded rectangular element. Three different discretizations are used for the analysis, namely  $2 \times 2$ , and  $4 \times 4$ . The finite element results are compared with the analytical results, for simply supported plates in Table 12.

Next the same laminated plate but with fully clamped boundary condition, as an example, is analyzed, as it does not allow analytical solution. Of course laminates with other boundary conditions may be analyzed with the finite element method developed herein. The results are obtained by using an 8-noded rectangular element with a  $4 \times 4$  mesh. Table 13 shows the results obtained. The vibration suppression characteristics are shown in Fig. 11. The results presented here are in agreement with those obtained for beams by Reddy and Barbosa (2000).

## 6. Conclusions

Analytical solution for simply supported plates and finite element solutions of composite plates with smart material layers embedded in them are presented in this study. The third-order plate theory is used to study vibration suppression characteristics. The analytical solution is based on the Navier solution procedure. The velocity feedback control is used. The displacement finite element model is developed with eight degrees of freedom ( $w_0, w_{0,x}, w_{0,y}, w_{0,xy}, \phi_x, \phi_y$ ) per node.

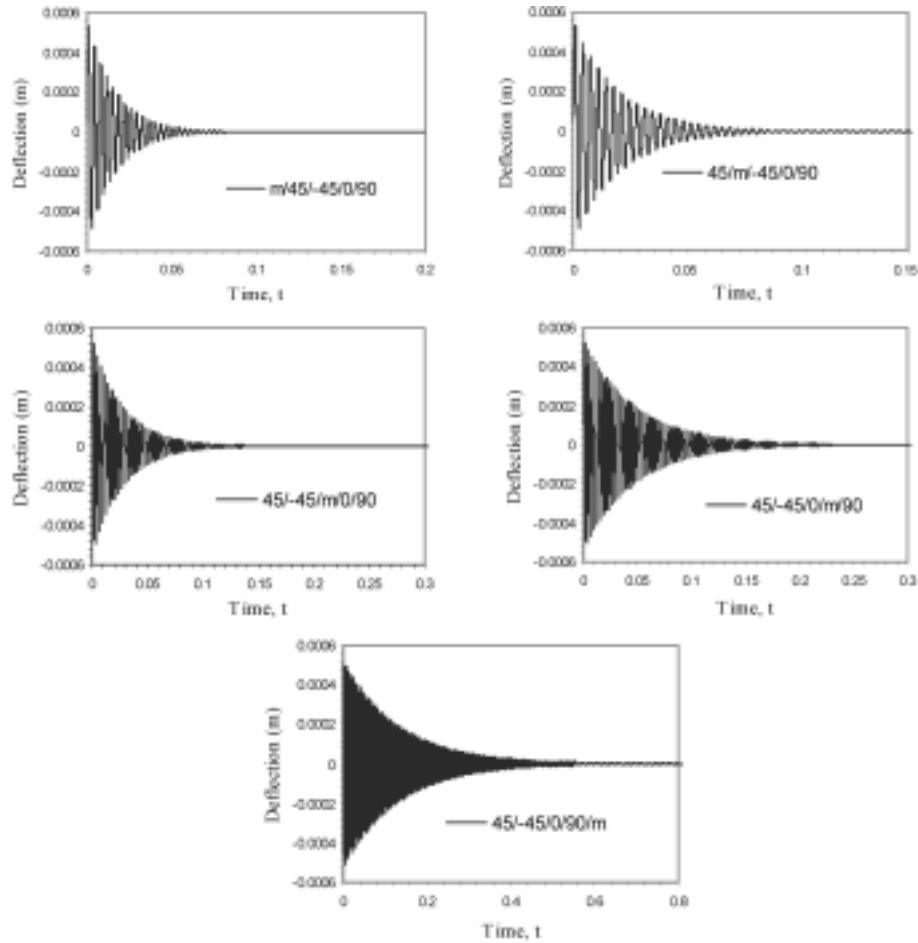


Fig. 11 Vibration suppression characteristics of fully clamped CFRP laminate

The smart material used in this study to achieve vibration suppression of laminated composite plates is the Terfenol-D magnetostrictive material. The vibration suppression characteristics of laminated plates are studied for a number of different cases and the results are presented in tables and figures. The behavior of composite plates with embedded magnetostrictive layers for different kinds of structural material has been studied. The suppression characteristics have been found to be similar for materials having similar  $E_1/E_2$  ratios. The effect of placing the smart material layer at various laminate positions with respect to the neutral axis of the plate has been studied. It has been found that there is maximum vibration suppression when the smart material layers are placed farthest from the neutral axis, which creates larger bending by the smart material layer. It has also been found that using thinner smart material layers have better vibration attenuation characteristics. The effect of using different values of the feedback coefficient has also been studied. It is observed that for a lower value of the feedback coefficient the time taken to suppress the vibration is longer. This is expected, as the amount of actuation done by the smart material layer onto the composite plate is less as the feedback value is less. As pointed out by Yang and Huang (1998), placing actuating/sensing layers symmetrically may not be the best choice to achieve optimal control of a

structure.

## Acknowledgement

The support of this research by Grant DAAD19-01-1-0483 from the Army Research Office (ARO) is gratefully acknowledged.

## References

- Anders, W.S., Rogers, C.A., and Fuller, C.R. (1991), "Control of sound radiation from shape memory alloy hybrid composite panels by adaptive alternate resonance tuning," *AIAA J.*, 365-376.
- Anjanappa, M., and Bi, J. (1994a), "A theoretical and experimental study of magnetostrictive mini actuators," *Smart Mater. and Struct.*, **1**, 83-91.
- Anjanappa, M., and Bi, J. (1994b), "Magnetostrictive mini actuators for smart structural application," *Smart Mater. and Struct.*, **3**, 383-390.
- Bailey, T., and Hubbard, J.E. (1985), "Distributed piezoelectric polymer active vibration control of a cantilever beam," *AIAA J.*, **8**, 605-611.
- Baz, A., Imam, K., and McCoy, J. (1990), "The dynamics of helical shape memory actuators," *J. Intelligent Mater. Systems and Struct.*, **1**, 105-133.
- Bryant, M.D., Fernandez, B., and Wang, N. (1993), "Active vibration control in structures using magnetostrictive Terfenol with feedback and/or neural network controllers," *J. Intelligent Mater. Systems and Struct.*, **4**, 484-489.
- Bailey, T., and Hubbard, J.E. (1985), "Distributed piezoelectric polymer active vibration control of a cantilever beam," *AIAA J.*, **8**, 605-611.
- Choi, Y., Sprecher, A.F., and Conrad, H. (1990), "Vibration characteristics of a composite beam containing electrorheological fluid," *J. Intelligent Mater. Systems and Struct.*, **1**, 91-104.
- Crawley, E.F., and Luis, J.D. (1987), "Use of piezoelectric actuators and elements of intelligent structure," *AIAA J.*, **25**, 1373-1385.
- Cross, L.E. and Jang, S.J. (1988), "Electrostrictive materials", in R.C. Pohanka and P.L. Smith (eds.), "Recent advances in piezoelectric ceramics," *Electronic Ceramics, Properties, Devices, and Applications*, ed. by L.M. Levinson, Marcel Dekker, Inc., New York, 129-137.
- Eda, H., Kobayashi, T., Nakamura, H., and Akiyama, T. (1995), "Giant magnetostriction compounds with structure textured by resin bound on giant magnetostriction fine powder in magnetic field and its actuator," *Transactions of Japanese Society for Mechanical Engineering, Series C*, **61**, 168-17.
- Goodfriend, M.J., and Shoop, K.M. (1992), "Adaptive characteristics of the magnetostrictive alloy, Terfenol-D, for active vibration control," *J. Intelligent Mater. Systems and Struct.*, **3**, 245-254.
- Krishna Murty, A.V., Anjanappa, M., and Wu, Y.-F. (1997), "The use of magnetostrictive particle actuators for vibration attenuation of flexible beams," *J. Sound and Vibration*, **206**, 133-149.
- Krishna Murty, A.V., Anjanappa, M., Wu, Y.-F., Bhattacharya, B., and Bhat, M.S. (1998), "Vibration suppression of laminated composite beams using embedded magnetostrictive layers," *Journal A-S*, **78**, 38-44.
- Maugin, G.A. (1988), *Continuum Mechanics of Electromagnetic Solids*, NorthHolland, The Netherlands.
- Newnham, R.E. (1993), "Ferroelectric sensors and actuators: Smart ceramics", *Ferroelectric Ceramics*, Setter, N. and Colla, E. L., eds., 363-380.
- Pratt, J.R., and Flatau, A.B. (1995), "Development and analysis of self-sensing magnetostrictive actuator design," *J. Intelligent Mater. Systems and Struct.*, **6**, 639-648.
- Reddy, J.N. (1984a), "A simple higher-order theory for laminated composite plates." *J. Appl. Mech.*, **51**, 745-752.
- Reddy, J.N. (1984b), *Energy and Variational Methods in Applied Mechanics*, Wiley, New York.

- Reddy, J.N. (1997), *Mechanics of Laminated Composite Plates: Theory and Analysis*, CRC Press, Boca Raton, Florida.
- Reddy, J.N. (1999a), "On laminated composite plates with integrated sensors and actuators," *Eng. Struct.*, **21**, 568-593.
- Reddy, J.N. (1999b), *Theory and Analysis of Elastic Plates*, Taylor & Francis, Philadelphia, Pennsylvania.
- Reddy, J.N. and Barbosa, J.A. (2000), "Vibration suppression of laminated composite beams," *Smart Mater. and Struct.*, **9**, 49-58.
- Uchino, K. (1986), "Electrostrictive actuators: Materials and applications," *Cer. Bull.*, **65**, 647-652.
- Yang, S.Y. and Huang, W.H. (1998), "Is a collocated piezoelectric sensor/actuator pair feasible for an intelligent beam?" *J. Sound and Vibration*, **216**(3), 529-538.
- Yellin, J.M., and Shen, I.Y. (1996), "Integration and design of piezoelectric elements in intelligent structures," *J. Intelligent Mater. Systems and Struct.*, **6**, 733-743.